JOURNAL OF OPTOELECTRONICS AND ADVANCED MATERIALS Vol. 11, No. 3, March 2009, p. 289 – 295

Optical properties of Sol-Gel prepared nano ZnO. The effects of aging period and synthesis temperature

A. ESMAIELZADEH KANDJANI*, A. SHOKUHFAR, M. FARZALIPOUR TABRIZ[a], N. A. AREFIAN[a], M. R. VAEZI[a]
Department of Material Science and Engineering, Faculty of Mechanical Engineering, K. N. Toosi University of Technology, Tehran, Iran
[a]*Materials and Energy Research Center (MERC), Karaj, Iran.*

In present work zinc Oxide (ZnO) nanoparticles were synthesized via Sol-Gel method in different temperatures and aging periods. The structures and morphologies of obtained nanoparticles were investigated via X-ray Diffractometer (XRD) and Transition Electron Microscope (TEM), respectively. The optical band gaps were estimated from Uv-Vis analyses. The results show high dependence of optical band gap to the synthesis conditions. The effects of these parameters on the band gap were investigated based on produced internal microstrains in the obtained zinc oxide structure. The band gap increase drastically with increase in synthesis duration. By decrease in sol-gel temperature the band gap shows a slight decrease.

(Received August 16, 2008; accepted March 19, 2009)

Keywords: ZnO, Sol-Gel, Band gap, internal microstrain, Urbach energy

1. Introduction

Semiconductor nano-materials, have been receiving lots of researchers' attention nowadays. Among these materials, zinc oxide due to its interesting properties and various morphologies has become one of the most attractive nanomaterials for research objectives. Zinc oxide has a wide band gap of 3.3 eV (at bulk state), low resistivity and high transparency in the visible light wave lengths and high light trapping characteristics and also a large exciton binding energy (60 meV) [1], which ensures its efficient ultraviolet (UV) emission up to room temperature [2]. The room temperature electron hole mobility in ZnO single crystals is about 200 $cm^2/V.s$ [3]. Hexagonal wurtzite (a=3.25Å and c=5.12Å) is the main stable crystal structure of ZnO at room temperature [4].

The properties of nano ZnO have made it applicable in UV-Light emitters, varistors, transparent high power electronics, gas sensors, etc [5]. Many approaches have been used for obtaining ZnO nanoparticles, including: Hydrothermal [6], Solvothermal [7], Reverse micelles [8], Sol-gel [9], Direct chemical synthesis [10], Sonochemical [11], etc.

Among these methods, Sol-Gel is one of the well known methods due to its easy procedure, easy control of film thickness, low-cost processing and coating ability of large complex shapes. Many parameters, including temperature, medium pH, aging period, amount and type of modifier and hydrolysis agent, can influence the properties of synthesized nanoparticles' beside their size and morphologies [12]. In present work, an attempt is made to investigate about the effects of aging time and synthesis temperature on the structure, crystallite size and optical band gap of zinc oxide nanoparticles.

2. Experimental

2.1. Materials

$Zn(Ac)_2.2H_2O$, Triethanolamin (TEA) and Ethanol were purchased from Merck and used as received.

2.2. Synthesis

5 different samples were synthesized in present work which their synthesis conditions are listed in Table 1.

Table 1. Synthesis variables.

Sample	Sol-Gel period (min)	Temperature (°C)
Z-1	20 min	60
Z-2	40 min	60
Z-3	60 min	60
Z-4	40min	40
Z-5	40min	20

First, based on the experiment conditions as listed in Table 1, 0.1molar $Zn(Ac)_2$ dissolved in 25ml distilled water for 30 min while in another vessel, TEA was dissolved in 25ml absolute ethanol [weight ratio of $\left(Zn(Ac)_2 / TEA\right)=1$]. Both vessels were kept at 40°C by using heating cooling bath. Then the vessels temperature was adjusted to desired temperature. After obtaining white solution, the prepared samples were gathered and dried at 60°C for 24hr. At last all samples were calcinated in 400°C for 1hr.

2.3. Analyses

The crystallographic structure of materials was studied using Siemens D-5000 X-ray diffractometer (XRD) with Cu-Kα radiation (λ= 0.154178 nm). Morphology of particles was studied by Transmission Electron Microscopy (Philips CM200). The optical properties were studied by UV–Vis spectrometry (Aquarius-CECIL CE9500).

2.4. Band gap and Crystallite size estimations

Absorption coefficients of colloidal ZnO suspension (α, cm^{-1}) have been calculated using the following equation [13]:

$$\alpha = 2303\left(\frac{D.\rho}{C.l}\right) \quad (1)$$

where, D is the optical density of a solution, ρ is the density of bulk ZnO crystals ($5.606\frac{g}{cm^3}$) [14], C is the ZnO concentration ($\frac{g}{cm^3}$) and l is the optical path (cm).

Further the median crystallite sizes of particles were investigated from the full width at half maximum (FWHM) of the highest diffraction peaks using the Debye–Scherrer formula [15]:

$$D = \frac{k\lambda}{\beta\cos\theta} \quad (2)$$

Where D is the mean crystallite size; k is a grain shape dependent constant (here assumed to be 0.89 for spherical particles); λ is the wavelength of the incident beam; θ is the Bragg reflection peak; and β is the full width of half maximum.

The internal micro strains of samples has been estimated using Williamson-Hall relation [16]:

$$\beta\cdot Cos\theta = \frac{k\lambda}{D} + \varepsilon\cdot Sin\theta \quad (3)$$

Where β is full width at half maximum (FWHM) of (100), (002), (101), (102) and (103) planes, k is the Scherrer constant, D is mean crystallite size, λ is the wavelength of irradiated X-Ray, θ is the Bragg angle and ε is the internal microstrain.

3. Results and discussion

3.1. Assigning band gap

Absorption coefficient, $\alpha(\lambda)$, of semiconductors is given by the following expression [17]:

$$\alpha = A\frac{(h\nu - E_g)^n}{h\nu} \quad (4)$$

where A is coefficient of the given electronic transition probability and n is equal to 0.5 and 2 for allowed direct and indirect transitions and 1.5 and 3 in case of forbidden direct and indirect transitions, respectively. Equation (5) which is derivated from expression (4), has a break point at $h\nu = E_g$ (Fig. 1b). Using this function precise determination of E_g value is possible.

$$\frac{d[\ln(\alpha\cdot h\nu)]}{d(h\nu)} = \frac{n}{h\nu - E_g} \quad (5)$$

Absorption spectra of ZnO nanoparticles (as in Fig. 1a) have been found to be linear in the $\ln(\alpha\cdot h\nu)$ vs. $\ln(h\nu - E_g)$ coordination (Fig. 1c). The slope of this line as shown in Fig. 1c (n in the Eq. (4)) is equal to 0.50 ± 0.02. Hence, the absorption of ZnO nanocrystals originates from the allowed direct interband electronic transitions.

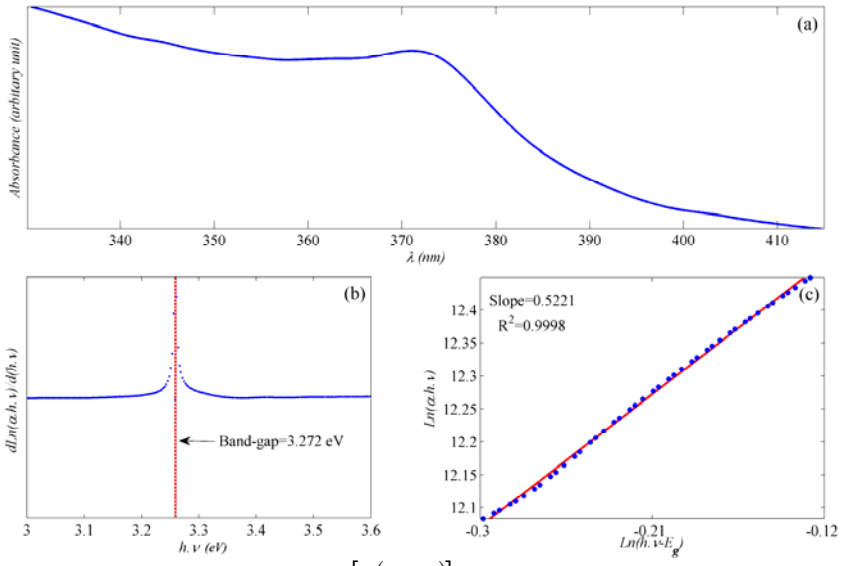

Fig 1. a) Absorption spectra of sample Z-3. b) $\frac{d[\ln(\alpha\cdot h\nu)]}{d(h\nu)}$ *vs.* $h\nu$ *for estimation of Z-3 sample band gap. c)* $\ln(\alpha\cdot h\nu)$ *vs.* $h\nu$ *for determination of transition type.*

The absorption coefficient α near band edge varies exponentially with photon energy. We can assume that the spectral dependence of the absorption edge is in accordance to Urbach formula [18]:

$$\alpha(h\nu)=\alpha_0 \cdot \exp\left[\frac{(h\nu)}{E_0}\right] \quad (6)$$

where α_0 is the Urbach absorption at the edge and E_0 is the Urbach energy width which is weakly dependant on temperature and believed to be a function of the structural disorder. The exponential dependence of the absorption on $h\nu$ in the Urbach region ($h\nu < E_g$) is due to the perturbation of the parabolic density of the states at the band edge – increasing structural disorder results in an increase in E_0 [19]. E_0 values were estimated from the slopes of the linear plot of $ln\alpha$ against $h\upsilon$ as shown in Fig. 2 for sample Z-2.Several factors are responsible for Urbach band tail including carrier-impurity interaction, carrier-phonon interaction, structural disorder, etc. Basically this parameter includes the effects of all possible defects [20-21].

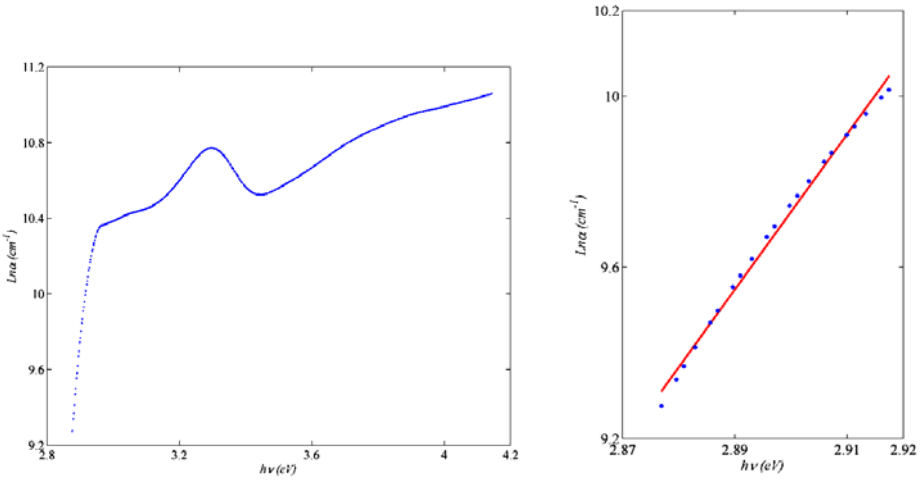

a b

Fig. 2 a) Variations of lnα vs. hυ for sample Z-2, b) Urbach tail of sample Z-2, estimated by means of least square best fitting procedure.

3.1. Sol-Gel process in present of TEA

The mechanisms of ZnO Sol-Gel synthesis with assistance of TEA can be described as below reactions.

At first step, the $Zn(Ac)_2$ is hydrolyzed in absolute ethanol as it is solved. The positively charged part of complex, bonds with TEA in the second step. The first and second reactions offer an element of hydrolysis, dehydration and polycondensation. Finally remained molecular structures join with each other and the sol is constructed by joining them together by hydrogen bonds. By increasing the temperature in drying process, these complexes are broken. This thermolysis results in formation of ZnO particles [22-23].

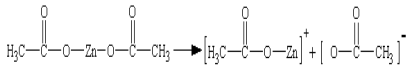

(7)

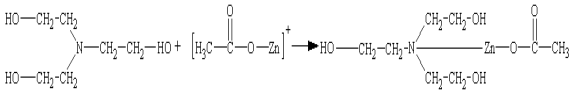

(8)

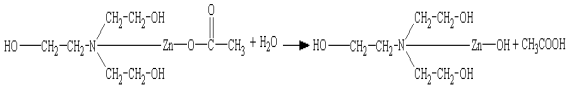

(9)

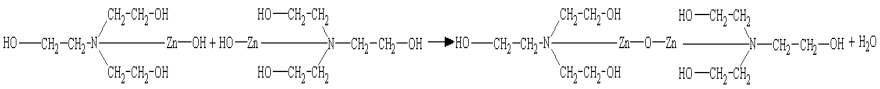

(10)

TEM image of sample Z-2 is shown in Fig. 3. As it can be seen in this image, the morphology of the obtained ZnO is semi spherical. The morphologies of other samples are very similar to Z-2; the only difference is particle size

distribution. The SAED analysis shows crystalline ZnO structure.

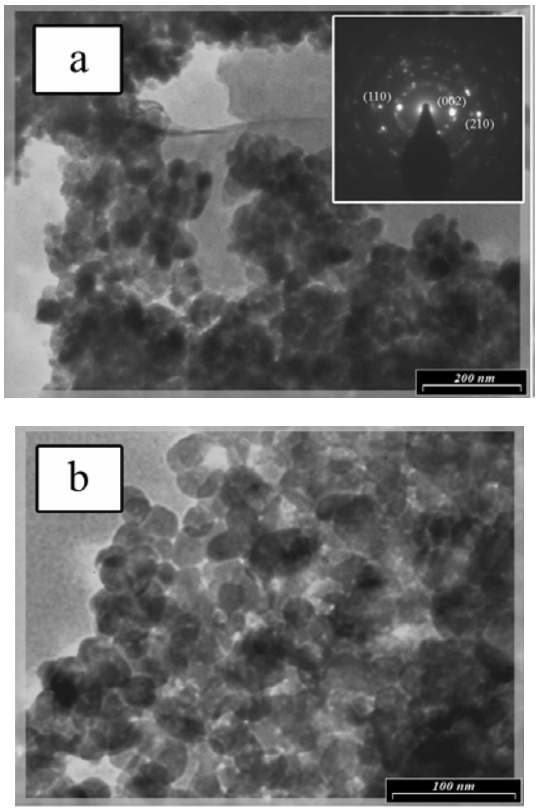

Fig. 3TEM image of sample Z-2in different magnifications; corresponding SAED pattern is shown in inset figure.

3.2. Effects of aging period

XRD patterns of samples Z-1, Z-2 and Z-3 are shown in Fig. 4. All peaks are attributed to wurtzite ZnO (JCPDF 36-1451) and no peaks of other crystalline phases were detected. As shown in This Figure, (002) planes have highest intensity and the intensity order of peaks is similar in these samples. But by increase in Sol-Gel aging period, width and height of the peaks are changed.

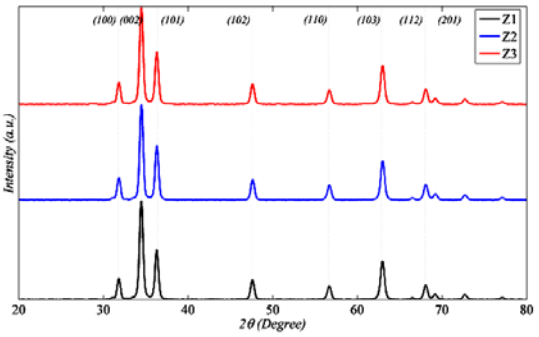

Fig. 4 XRD pattern of samples Z-1, 2 and 3.

From Eq. (2) the mean crystallite sizes of the samples are estimated as shown in Fig. 5. Increasing the Sol-Gel aging period results in the grain growth of the zinc oxide. This can be due to coarsening process driven by difference in solubility between surfaces and different radii of particles curvature. Particles have positive radii of curvature so they are more soluble than flat plates of same material. The smaller particles dissolve and solute precipitates onto larger particles. This mechanism is called Ostwald ripening whereby particles grow in size and decrease in number as highly soluble small particles dissolve and reprecipitate on larger, less soluble nuclei. Growth stops when the difference in solubility between the smallest and largest particles becomes only a few ppm. This process tends to increase of crystallite size of sample [24].

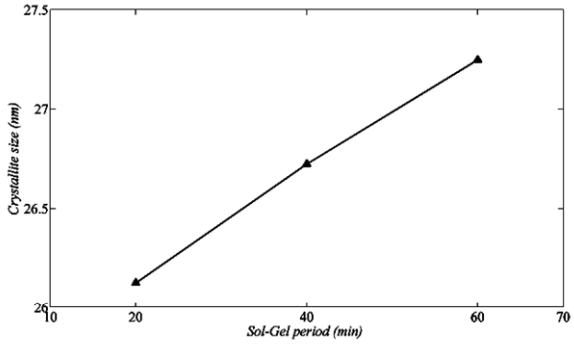

Fig. 5 The crystallite growth of zinc oxide with Sol-Gel time.

The UV absorbance spectra of these samples are illustrated in Fig. 6. The absorbance spectra of obtained ZnO samples have an intense change in 360 to 400nm range. A large shoulder in this is visible in the absorbance spectra. This exitonic peak is related to the quantum confinement effect due to nanoscopic size of the crystallites [25].

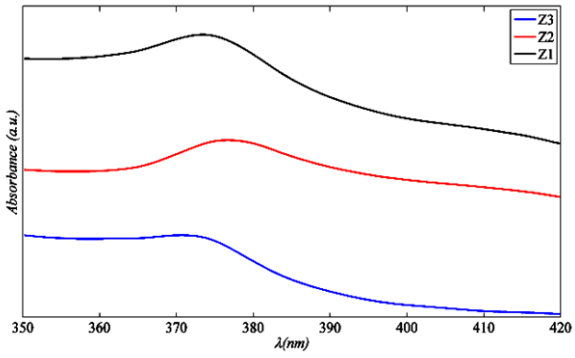

Fig. 6. UV-Vis absorbance spectra for samples Z-1, 2 and 3.

According to Fig. 6 and from Eq. (4), band gap values of samples are estimated as shown in Fig. 7. In comparison

with band gap value of bulk unstrained ZnO i.e. 3.30eV, all samples have less band gap values.

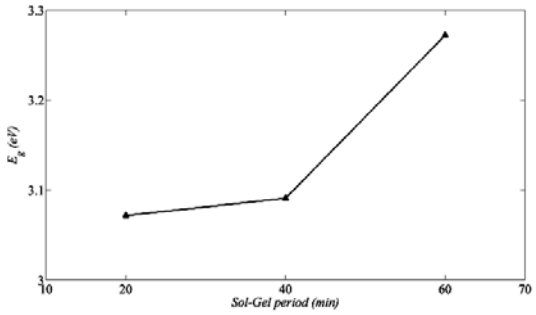

Fig. 7. Dependence of band gap to sol-gel period.

This might be due to the strain arising from chemical synthesis of ZnO and short duration of calcinations and annealing. These micro-strains highly influence the optical band gap of material [26]. The micro-strain in samples estimated from Eq. (3), decrease by increasing Sol-Gel duration as shown in Fig. 8. The strained regions in materials tend to solute faster than stress-free areas so solution-precipitation process results in lowering the total micro-strains in prepared samples. This phenomenon can affect the E_0 of the samples as shown in Fig. 9. E_0 values decrease as the strains in the materials decrease which can subsequently influence the optical properties of the material.

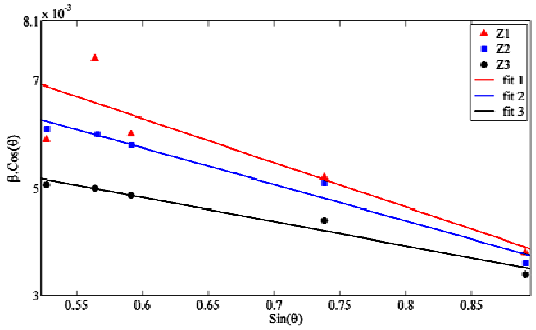

Fig. 8 Internal microstrain changes Sol-Gel time.

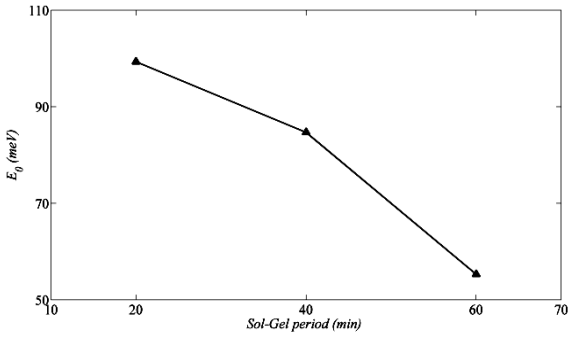

Fig. 9 Dependence of Urbach energy width to Sol-Gel period.

According to resulted values for micro-strains and crystallite size of the samples, by prolonging aging process, the band gap values increase. These values are approaching to bulk band gap value of ZnO.

3.5. Effect of procedure temperature

Fig. 10 shows XRD patterns of samples Z-2, Z-4 and Z-5 which shows the structures of obtained zinc oxide nanoparticles with changes of synthesis duration. In these synthesized materials same as previous samples, all peaks are attributed to wurtzite ZnO (JCPDF 36-1451) and no peaks of other crystalline phases were detected.

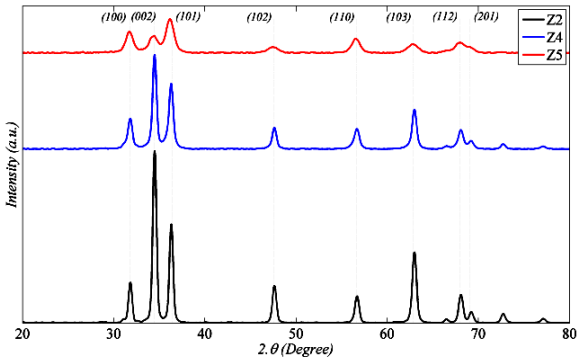

Fig. 10 XRD patterns of samples Z-2, 4 and Z-5.

The most important point in structure of these zinc oxides is dependence of its XRD peaks intensities to synthesis temperature. As it can be seen in Fig. 10 the most intensive peak in XRD pattern of the sample prepared in 20°C belongs to (101) planes while this characteristic change by increasing synthesis temperature and in 60°C the highest peak belongs to (002) planes of zinc oxide. These changes can offer a different growth method which is highly depended to thermodynamical and kinetical conditions [27].

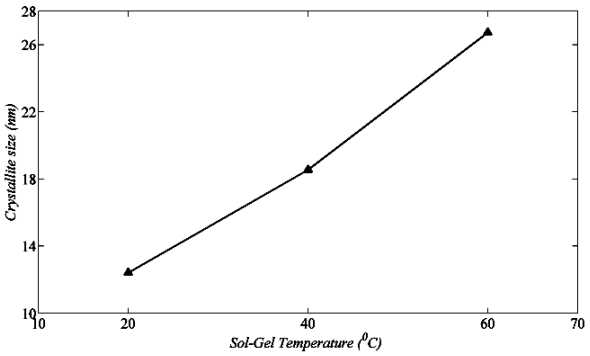

Fig. 11 The crystallite growth of zinc oxide with synthesis temperature.

From Eq. (2) the mean crystallite sizes of the samples are estimated as shown in Fig. 11. Since the condensation reaction is exothermic, increase of temperature increase

the solubility of materials so accelerates the grain growth by Ostwald ripening mechanism [27].

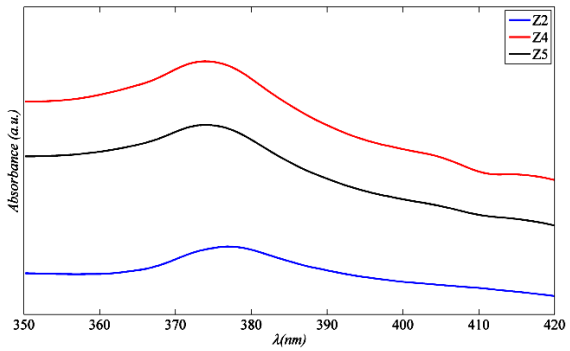

Fig. 12 UV-Vis absorbance spectra for samples Z-2, 4 and 5.

According to Fig. 12 band gap values of samples are estimated as shown in Fig. 13. A red shift occurs in these samples in comparison with band gap value of bulk unstrained ZnO.

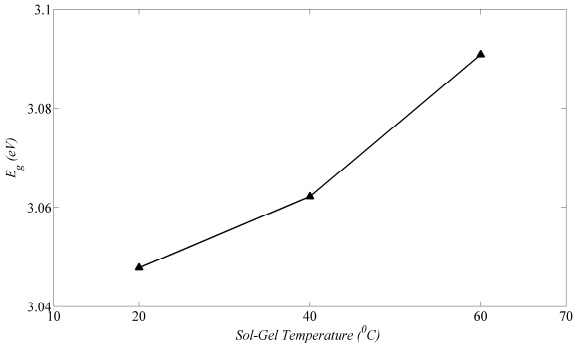

Fig. 13 Dependence of band gap to sol-gel temperature.

The micro-strain in samples estimated from Eq. (3), decrease by increasing Sol-Gel duration as shown in Fig. 14. As expected, the amounts of internal microstrain increase by decrease in synthesis temperature. This can be explained due to providing less energy in ambient temperatures for dissolving the strained regions in materials.

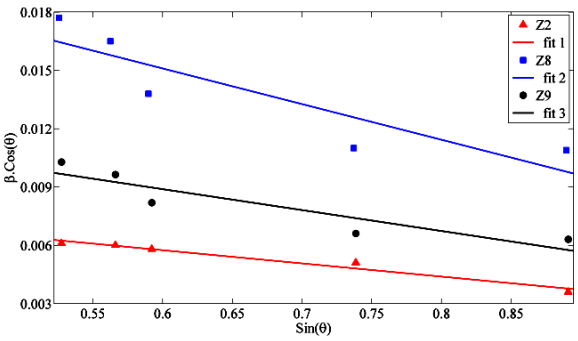

Fig. 14 Internal microstrain changes Sol-Gel temperature.

This phenomenon can affect the E_0 of the samples as shown in Fig. 15. E_0 values decrease as the strains in the materials decrease which can subsequently influence the optical properties of the material.

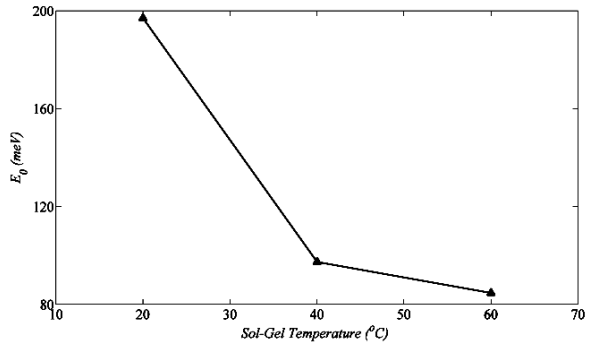

Fig. 15 Dependence of Urbach energy width to Sol-Gel temperature.

The obtained properties of the materials are listed in Table 2 for better understanding.

Table 2. The obtained properties of the synthesized samples.

Sample	Mean crystallite size (nm) [±0.05]	Band gap (eV) [±0.05]	Urbach energy (meV) [±0.5]
Z-1	26.12	3.07	97.3
Z-2	26.72	3.09	84.7
Z-3	27.25	3.27	55.28
Z-4	17.54	3.05	99.34
Z-5	12.41	3.03	196.96

As shown in Table 2, the mean crystallite sizes of obtained nanoparticles changes drastically with change in synthesis temperature than synthesis duration. Producing smaller particles tends to expand the obtained band gap [28]. On the other hand due to lower synthesis temperature, the interior strains of the samples are much more than the other samples. These phenomena compete with each other and thus the band gap changes slightly with temperature variation.

4. Conclusion

In present work, ZnO nanoparticles were synthesized via Sol-Gel method. The effects of the synthesis temperature and aging duration on the optical band gap were investigated. The crystallite size and the band gap of obtained nanoparticles vary from 12.41nm to 27.25nm and 3.03eV to 3.27eV, respectively. Also the Urbach widths of ZnO nanoparticles were varied from 55.28meV to 196.96meV. The results show that the temperature has the

highest influence on the crystallite size and internal microstrain which is lead to expand in Urbach energy width. Thus, the microstrain and quantum size effects are in competition with each other and these two phenomena must be considered together for investigating on optical band gap of semiconductors.

Reference

[1] L. Xu, Y. Su, Y.Q. Chen, H.H. Xiao, L.A. Zhu, Q. T. Zhou, S. Li, J. Phys. Chem. B **110**, 6637 (2006).

[2] R. Deng, X. T. Zhang, J. Lumin. **128**, 1442 (2008).

[3] A.R. Hutson, Phys. Rev. **108**, 222 (1957).

[4] D. P. Norton, M. Ivill, Y. Li, Y.W. Kwon, J. M. Erie, H.S. Kim, K. Ip, S.J. Pearton, Y.W. Heo, S. Kim, B. S. Kang, F. Ren, A.F. Hebard, J. Kelly, Thin Solid Films **496**, 160 (2006).

[5] S. J. Pearton, D.P. Norton, K. Ip, Y.W. Heo, T. Steiner, Prog. Mater. Sci. **50,** 293 (2005).

[6] Y.H. Ni, X.W. Wei, J.M. Hong, Y. Ye, Mat. Sci. Eng. B **121,** 42 (2005).

[7] C. Wang, E. Shen, E. Wang, L. Gao, Z. Kang, C. Tian, Y. Lan, C. Zhang, Mater. Lett. **59,** 2867 (2005).

[8] T. Hirai, Y. Asada, J. Colloid. Interf. Sci. **28,** 184 (2005).

[9] M. Ristić, S. Musić, M. Ivanda, S. Popović, J. Alloy. Compd. **397,** L1 (2005).

[10] C. Wu, X. Qiao, J. Chen, H. Wang, F. Tan, S. Li, Mater. Lett. **6,** 1828 (2006).

[11] A. Esmaielzadeh Kandjani, M. Farzalipour Tabriz, B. Pourabbas, Mater. Res. Bull. **43,** 645 (2008).

[12] L. Klein, Sol-Gel Technology for Thin Films, Fibers, Performs, Electronics, and Specialty Shapes, Park Ridges, (1998).

[13] S. V. Gaponenko, Optical Properties of Semiconductor Nanocrystals. Cambridge: University Press, (1996).

[14] Ü. Özgür, Ya. I. Alivov, C. Liu, A. Teke, M. A. Reshchikov, S. Doğan, V. Avrutin, S.-J. Cho, H. Morkoç, J. Appl. Phys. **98**, 041301 (2005).

[15] B. D. Cullity, Elements of X-ray Diffraction, Second edition, Addison-Wesley Company, U.S.A (1978).

[16] C. Suryanaryana, M. G. Norton, X-ray diffraction: A practical approach, Plenum Press, U.S.A., (1998).

[17] J. J. Ramsden, M. Gratzel, J. Chem. Soc., Faraday Trans. **80**, 919 (1984).

[18] F. Urbach, Phys. Rev. **92,** 1324 (1953).

[19] N. B. Chen, H. Z. Wu, D. J. Qiu, T. N. Xu, J. Chen, W. Z. Shen, J. Phys. Condens. Matter. **16**, 2973 (2004).

[20] V. Srikant, D.R. Clarke, J. Appl. Phys. **81**, 6357 (1997).

[21] J. I. Pankove, Phys. Rev. A **140**, 2059 (1965).

[22] L. Znaidi, G.J.A.A. Soler Illia, S. Benyahia, C. Sanchez, A.V. Kanaev: Thin Solid Films **428,** 257 (2003).

[23] Z. Liu, Z. Jin, W. Li, J. Qiu, Mater. Lett. **59,** 3620 (2005).

[24] O. Sohnel, J. W. Mullin, J. Colloid. Interf. Sci. **123**, 43 (1988).

[25] E. A. Meulenkamp, J. Phys. Chem. B **102**, 5566 (1998).

[26] V. Srikanth, D.R. Clarke, J. Appl. Phys. **81**, 6357 (1997).

[27] C. J. Binker, G. W. Scherer, Sol-Gel Science: The physics and Chemistry of Sol-Gel Processing, Academic Press Inc., UK, (1990).

[28] M. Li, J.C. Li, Mater. Lett. **60**, 2526 (2006).

*Corresponding author: MSTGAhmad@Gmail.com